OGLE-2017-BLG-0373Lb: A Jovian Mass-Ratio Planet Exposes A New Accidental Microlensing Degeneracy

J. Skowron[1], Y.-H. Ryu[2], K.-H. Hwang[2],

and

A. Udalski[1], P. Mróz[1], S. Kozłowski[1], I. Soszyński[1], P. Pietrukowicz[1], M. K. Szymański[1], R. Poleski[1,3], K. Ulaczyk[1], M. Pawlak[1], K. Rybicki[1], P. Iwanek[1]
(OGLE Collaboration)
M. D. Albrow[4], S.-J. Chung[2,5], A. Gould[2,3,6], C. Han[7], Y. K. Jung[8], I.-G. Shin[8], Y. Shvartzvald[9,†], J. C. Yee[8], W. Zang[10,11], R. W. Zhu[12], S.-M. Cha[2,13], D.-J. Kim[2], H.-W. Kim[2], S.-L. Kim[2,5], C.-U. Lee[2,5], D.-J. Lee[2], Y. Lee[2,13], B.-G. Park[2,5], R. W. Pogge[3]
(KMTNet Collaboration)

[1] *Warsaw University Observatory, Al. Ujazdowskie 4, 00-478 Warszawa, Poland*

[2] *Korea Astronomy and Space Science Institute, Daejon 34055, Korea*

[3] *Department of Astronomy, Ohio State University, 140 W. 18th Ave., Columbus, OH 43210, USA*

[4] *University of Canterbury, Department of Physics and Astronomy, Private Bag 4800, Christchurch 8020, New Zealand*

[5] *Korea University of Science and Technology, Daejeon 34113, Korea*

[6] *Max-Planck-Institute for Astronomy, Königstuhl 17, 69117 Heidelberg, Germany*

[7] *Department of Physics, Chungbuk National University, Cheongju 28644, Republic of Korea*

[8] *Harvard-Smithsonian CfA, 60 Garden St., Cambridge, MA 02138, USA*

[9] *Jet Propulsion Laboratory, California Institute of Technology, 4800 Oak Grove Drive, Pasadena, CA 91109, USA*

[10] *Physics Department and Tsinghua Centre for Astrophysics, Tsinghua University, Beijing 100084, China*

[11] *Department of Physics, Zhejiang University, Hangzhou, 310058, China*

[12] *Canadian Institute for Theoretical Astrophysics, University of Toronto, 60 St George Street, Toronto, ON M5S 3H8, Canada*

[13]*School of Space Research, Kyung Hee University, Yongin, Kyeonggi 17104, Korea*

[†]*NASA Postdoctoral Program Fellow*

ABSTRACT

We report the discovery of microlensing planet OGLE-2017-BLG-0373Lb. We show that while the planet-host system has an unambiguous microlens topology, there are two geometries within this topology that fit the data equally well, which leads to a factor 2.5 difference in planet-host mass ratio, i.e., $q = 1.5 \times 10^{-3}$ versus $q = 0.6 \times 10^{-3}$. We show that this is an "accidental degeneracy" in the sense that it is due to a gap in the data. We dub it "the caustic-chirality degeneracy". We trace the mathematical origins of this degeneracy, which should enable similar degenerate solutions to be easily located in the future. A Bayesian estimate, based on a Galactic model, yields a host mass $M = 0.25^{+0.30}_{-0.15} M_\odot$ at a distance $D_L = 5.9^{+1.3}_{-1.95}\,\mathrm{kpc}$. The lens-source relative proper motion is relatively fast, $\mu = 9\,\mathrm{mas\,yr^{-1}}$, which implies that the host mass and distance can be determined by high-resolution imaging after about 10 years. The same observations could in principle resolve the discrete degeneracy in q, but this will be more challenging.

Subject headings: gravitational lensing: micro

1. Introduction

The interpretation of gravitational microlensing events is subject to a variety of discrete degeneracies, which can be divided into two broad categories: intrinsic and accidental. Intrinsic degeneracies are generally rooted in symmetries of the lens equation. The most famous of these is the "close/wide" degeneracy between binary lens solutions having projected separations s (scaled to the angular Einstein radius θ_E) that approximately obey $s \leftrightarrow s^{-1}$. These were first discovered in the context of a theoretical study of planetary lensing in the high-magnification regime by Griest & Safizadeh (1998). Soon after, Dominik (1999) showed that they constituted the limiting form of a degeneracy that impacted binary lenses of all mass ratios and was rooted in a symmetry between a quadrupole expansion of the lens equation for $s < 1$ and a shear expansion for $s > 1$. An (2005) then found that this degeneracy continued at next order when he studied the lens equation still more deeply.

Another intrinsic degeneracy is the so-called "ecliptic degeneracy". Its origins were first studied mathematically by Smith et al. (2003), whose work was later extended in different

directions by Gould (2004) to the "jerk-parallax degeneracy" and by Skowron et al. (2011) to a discrete degeneracy involving four parameters in binary lensing.

On the other hand, there are also accidental degeneracies, i.e., those that do not derive from deep symmetries of the lens equation but rather from "accidental" alignments of magnification patterns arising from unrelated lens configurations. Very often, these magnification-pattern alignments are restricted to a limited domain, so that the degeneracy is easily broken if there are sufficient data in other regions of the light curve where this alignment fails. However, there are at least two degeneracies that can be quite intractable even though they are not rooted in the lens equation. One of these, discovered by Gaudi (1998), is between planetary events (two lenses one source, 2L1S) that lack detailed caustic crossings and binary-source events (1L2S). An especially complex example of this was discovered by Hwang et al. (2017), who found equally good 3L1S, 2L2S, and 1L3S solutions for OGLE-2015-BLG-1459. In the end, this degeneracy was resolved in favor of the triple source (1L3S) solution, but only because there were color data serendipitously available, and the 1L3S solution predicted strong chromatic effects while the others did not.

Another quite intractable (and also quite unexpected) degeneracy was recently found by Hwang et al. (2018) for OGLE-2017-BLG-0173 between two classes of "Hollywood" events in which the source is of order or larger than the planetary caustic. They showed that the "Cannae" and "von Schlieffen" topologies, in which the source fully or partially envelops the caustic, produced almost identical light curves. In fact, this degeneracy is not intrinsically intractable: the two models predict different light curves in regions where there are no data. Still, these predicted differences are remarkably small. The nature of this degeneracy is still not fully understood. Hwang et al. (2018) found that it did not apply to another Cannae Hollywood event OGLE-2005-BLG-390 (Beaulieu et al. 2006), while Udalski et al. (2018) found that it did apply to hypothetical events similar to OGLE-2017-BLG-0173 but with much lower mass ratio.

It is exceptionally important to identify as many classes of these degeneracies as possible so that the true solution is not missed and so that the cases for which there are multiple viable solutions with substantially different physical implications are recognized. For example, prior to the discovery of the jerk-parallax degeneracy, Alcock et al. (2001) found a microlens parallax solution for MACHO-LMC-5 that led to the conclusion of a luminous lens at a distance of 200 pc but with a mass well below the hydrogen-burning limit, which they regarded as quite remarkable. The second parallax solution was found by Gould (2004) accidentally, in the course of trying to reproduce this solution, and he proceeded to identify its mathematical nature within the framework of the Smith et al. (2003) formalism. Part of that work yielded an equation (made substantially more user-friendly by Park et al. 2004)

to predict the jerk-parallax counterpart once one solution is found. Hence, at this point, one can easily determine whether this degeneracy is present.

Similarly, a downhill approach could easily miss (and, actually, did originally miss) the Cannae solution to OGLE-2017-BLG-0173, being "blocked" by the "nearby" von Schlieffen solution. In fact, while these solutions are "nearby" in most lensing parameters, they differ by a factor ~ 2.5 in planet-host mass ratio. Indeed, Hwang et al. (2018) showed analytically that von Schlieffen mass ratios should generically be higher by a factor ~ 2. Hence, in the future, these degeneracies can be easily detected because if either the Cannae or von Schlieffen solutions are found, the parameters of the other can be approximately predicted.

Here we analyze OGLE-2017-BLG-0373 and show that it exhibits a previously unknown accidental degeneracy, which we dub "the caustic-chirality degeneracy". We investigate the origins of this degeneracy and show that it can easily appear in events for which half or more of the light curve traversing a planetary caustic is devoid of observational data.

2. Observations

OGLE-2017-BLG-0373 is at (RA,Dec) = (17:57:19.06,−31:57:06.2), corresponding to $(l, b) = (-1.31, -3.71)$. It was discovered and announced as a probable microlensing event by the OGLE Early Warning System (Udalski et al. 1994; Udalski 2003) at UT 15:04 23 March 2017. The event lies in OGLE-IV field BLG507 (Udalski et al. 2015), for which OGLE observations were at a cadence of $\Gamma = 0.4\,\mathrm{hr}^{-1}$ using their 1.3m telescope at Las Campanas, Chile.

The Korea Microlensing Telescope Network (KMTNet, Kim et al. 2016) observed this field from its three 1.6m telescopes at CTIO (Chile, KMTC), SAAO (South Africa, KMTS) and SSO (Australia, KMTA), in its two slightly offset fields BLG01 and BLG41, with a combined cadence of $\Gamma = 4\,\mathrm{hr}^{-1}$. However, the KMTA data are of substantially lower quality, and they do not contribute to characterizing the planetary anomaly. Hence, we do not use them. The event was identified as SAO41N0303.005729 by KMTNet.

The great majority of observations were carried out in the I band with occasional V-band observations made solely to determine source colors. All reductions for the light curve analysis were conducted using variants of difference image analysis (DIA, Alard & Lupton 1998), specifically Woźniak (2000) and Albrow et al. (2009).

3. Light Curve Analysis

3.1. Heuristic Analysis

Figure 1 shows the data, together with a point-lens model, for OGLE-2017-BLG-0373. With the exception of an anomaly lasting a total of just 0.3 days near $\mathrm{HJD}' \equiv \mathrm{HJD} - 2450000 = 7835$, the event appears to be a simple point-lens (Paczyński 1986) light curve, characterized by three parameters: the time of closest approach t_0, the impact parameter (normalized to θ_E) u_0, and the Einstein timescale t_E. The apparent amplitude is only $\Delta I \sim 0.3$ mag, but a priori one does not know whether this is because the event has an intrinsically low amplitude or is heavily blended. We exclude the anomaly and fit to a point lens, thereby finding $(t_0, t_\mathrm{eff}, t_\mathrm{E}) = [(7840.70, 4.73, 12.9) \pm (0.05, 0.22, 1.2)]$ days where $t_\mathrm{eff} \equiv u_0 t_\mathrm{E}$.

The entire light curve, with its clear caustic exit superposed on a Paczyński (1986) curve, is remarkably suggestive of Figure 1 from Gould & Loeb (1992), i.e., the original illustration of a planetary-caustic perturbation to a microlensing event. Because of this classic appearance, the event was immediately singled out for further analysis when it was noticed in the course of testing a "quick look" KMTNet pipeline to aid in the choice of *Spitzer* microlensing targets (Gould et al. 2016)[1].

However, in contrast to the Gould & Loeb (1992) figure (which was purely theoretical), the OGLE-2017-BLG-0373 light curve is "missing" its caustic entrance. For this reason, the light curve is actually roughly consistent with a remarkably wide range of binary-lens topologies. See Figure 2. A more detailed analysis shows that all but one of these five basic topologies is ruled out at the $\Delta\chi^2 \gtrsim 100$ level. Nevertheless, it is important to note that if the actual event had been generated by any of the other models shown in Figure 2, it would have appeared qualitatively the same to the eye, and so would have triggered the same investigation. Hence, it is crucial to explore all possible topologies, even when an event looks "obviously planetary".

We next undertake a heuristic analysis of the surviving topology, i.e., a planetary perturbation of the major image ($s > 1$), which is in fact the same as that illustrated by Gould & Loeb (1992). This analysis will frame the introduction of a new degeneracy within this topology.

The anomaly is offset from the peak by $\delta t = -6.2$ days. Hence, the angle of the source trajectory relative to the binary axis is $\alpha = \tan^{-1}(t_\mathrm{eff}/\delta t) = 143^\circ \pm 2^\circ$. The lens-source

[1]The event could not itself be targeted for *Spitzer* observations because it was already at baseline at the onset of the *Spitzer* campaign.

separation (normalized to $\theta_{\rm E}$) at the time of the anomaly is $u_{\rm caust} = \sqrt{t_{\rm eff}^2 + (\delta t)^2}/t_{\rm E} = 0.605 \pm 0.055$. Noting that $s - s^{-1} = u_{\rm caust}$ for major-image perturbations, we obtain $s = 1.35 \pm 0.03$.

To estimate the planet-host mass ratio q, we apply the formalism of Han (2006), specifically Section 3.1. He gives the caustic major and minor axes as $(\Delta\xi_c, \Delta\eta_c) = \sqrt{16q/(s^4 \mp s^2)} \rightarrow q^{1/2}(3.27, 1.76)$. Unfortunately, we do not have a very good estimate of the duration of the time that the source is inside the caustic, $\Delta t_{\rm caust}$, because there are no data from the caustic entrance. Nevertheless, there is a clear upper limit from the flat KMTC data at HJD$' = 7834.90$, and a plausible lower limit from the fact that the KMTS data are roughly flat HJD$' = 7834.45$. Hence we estimate, $0.6\,{\rm day} < \Delta t_{\rm caust} < 0.9\,{\rm day}$. The main difficulty in estimating q, however, is that it is hard to assess the geometry of the crossing given the fragmentary light curve. We do know that the angle is $\alpha \simeq 143^\circ$, which implies that the caustic is being crossed diagonally. Hence, the length of the transit will be substantially shorter than the major axis. We adopt the minor axis. We then obtain $q = [(\Delta t_{\rm caust}/t_{\rm E})/\Delta\xi_c]^2 \simeq 1 \times 10^{-3}$. Given the crude estimates of $\Delta t_{\rm caust}$ and of the geometry of the crossing, we consider that this should be accurate to a factor ~ 3. However, this exercise at least tells us that this is a Jovian mass-ratio planet.

Finally, we estimate the source self-crossing time $t_* = \rho t_E$, where $\rho \equiv \theta_*/\theta_{\rm E}$ and θ_* is the angular radius of the source. From Figure 1, the time from the peak to the end of the caustic exit is $\Delta t_{\rm exit} = 0.073\,{\rm days}$. From Figure 1 of Gould & Andronov (1999) this is related to self-crossing time by $t_* = \Delta t_{\rm exit} \sin\phi/1.7 = 1.0 \sin\phi\,{\rm hr}$, where ϕ is the angle between the source trajectory and the caustic. Because the source crosses the caustic diagonally, we can estimate $\sin\phi \sim 1$. Hence, $t_* \simeq 1\,{\rm hr}$ and $\rho \simeq 0.003$.

3.2. Numerical Analysis

We search for solutions in two stages. First we conduct a grid search over (s, q) space, in which these two parameters are held fixed, while the remaining five parameters $(t_0, u_0, t_{\rm E}, \rho, \alpha)$ are allowed to vary in a Monte Carlo Markov Chain (MCMC). The first four of these are seeded at the values derived in Section 3.1, while the last is seeded on a grid of six values. To evaluate the magnification, we use inverse ray shooting in and near the caustic (Kayser et al. 1986; Schneider & Weiss 1988; Wambsganss 1997) and multipole approximations (Pejcha & Heyrovský 2009; Gould 2008) elsewhere. In the second step, we seed each MCMC run with the parameters of the local minima identified in the first step. Figure 2. shows the models from these refined minima. As discussed in Section 3.1, there are five different models, each with very different topologies, that yield plausible likenesses

to the data. However, one of these is favored by $\Delta\chi^2 \gtrsim 100$ relative to the others, namely the major-image planetary-caustic model, which corresponds to the lens-system topology presented in the top right panel of Figure 2. In Table 1, we list the (s, q) and χ^2 of these five models.

Where do Models 1–4 fail? Figure 3 displays the residuals to the five models shown in Figure 2. All four failed topologies suffer from somewhat "wavy" residuals over many weeks. In the case of Model 2 and Model 4, this is punctuated by a severe discrepancy on the day following the caustic exit (and the day of the caustic exit for Model 4). However, Model 1 and Model 3 fail due to roughly one week periods of systematic residuals, centered on HJD$' \sim 7835$ and and ~ 7823, respectively.

In the above fitting process, the preferred topology has a well-localized minimum, which is given as "Local A" in Table 2. Note that the heuristic analysis of Section 3.1 quite accurately predicted all the parameters except q. This shows that the overall geometry (for the major-image planetary-caustic topology) is very well constrained by the gross features of the light curve. However, it leaves open the question of whether the specific value of q is actually correct.

Indeed, when we run a hotter chain (i.e., with error bars artificially inflated), we find that there are actually two neighboring minima. These have nearly identical χ^2 but differ in mass ratio q by a factor 2.5 (0.4 in the log). Figure 4 shows the models and caustic geometries of these two solutions. Table 2 gives the parameters for both models.

3.3. Origin of the Degeneracy

Why are there two solutions, rather than either one or many? At one level, the reason for multiple solutions is obvious from inspection of Figure 4: there are no data during or shortly after the caustic entrance. Even a few data points would have clearly distinguished between these models. However, this still does not explain why there are two solutions rather than many discrete solutions or a large continuous degeneracy.

To investigate this question, we employ the $\Delta\xi$ parameter introduced by Hwang et al. (2018) to analyze the degeneracy in the case of OGLE-2017-BLG-0173, the offset of the source trajectory from the planetary caustic,

$$\Delta\xi \equiv u_0 \csc\alpha - \xi_+(s); \qquad \xi_+(s) \equiv s - s^{-1}, \tag{1}$$

where $\xi_+(s)$ is the source position for which the major image coincides with the planet. Figure 5 shows $\Delta\chi^2$ as a function of position on the $(\log q, \Delta\xi)$ plane and can be directly

compared to Figure 4 of Hwang et al. (2018). This figure confirms what is already apparent by comparing the two caustic diagrams in Figure 4, namely that the source crosses the binary axis on opposite sides of the caustic center for the two models, and that it passes on the side closer to the host for the case of smaller q. However, it also shows that there is a $\Delta\chi^2 \sim 9$ "barrier" between the two solutions at about $\Delta\xi = -0.0075$.

Hence, we are led to ask why is the fit worse at this intermediate position? This is another way of asking why the degeneracy is two-fold? Apart from the duration of the caustic exit, $\Delta t_{\rm exit}$, the profile of a generic fold-caustic exit is basically set by three parameters: the post-caustic magnification A_0, the time of the exit, $t_{0,\rm caust}$, and the "strength" of the caustic, Z, i.e., $A(t) = A_0 + Z(t_{0,\rm caust} - t)^{-1/2}\Theta(t_{0,\rm caust} - t)$. The functional form of the caustic-exit data (in this case from KMTC) directly determine A_0, $t_{0,\rm caust}$, and $\Delta t_{\rm exit}$, which leaves only one degree of freedom: Z. The caustic strength Z generically peaks at the cusps and reaches a minimum somewhere between them along the fold caustic. Thus, for fixed q there are exactly two (or zero) positions along the fold caustic at which the predicted peak of the caustic exit matches the observed peak.

Of course, if one has chosen the correct q then it will be possible to find the other correct parameters so the magnification evolution everywhere correctly predicts the data. As the model moves away from this q, it will still be possible to find the remaining parameters so that the caustic exit is correctly predicted, but the resulting position of the caustic exit will create increasing tension with the profile in the interior of the caustic. In the present case, because of gaps in the data, particularly at the caustic entrance, the tension is entirely generated by mis-predicting the flux seen from KMTS near HJD$' = 7834.5$. That is, as q declines, the trajectory is driven closer to the cusp as it exits the fold caustic, which implies that it is also traveling closer to the (neighboring) fold caustic when it is interior to the caustic. This causes the predicted flux in the interior to be too high.

Initially, at the correct q, the alternate allowed point of caustic exit predicts a flux in the interior that is either too high or too low by some arbitrary amount. If it is too high, then as q is adjusted upward, the point of exit will be driven away from the cusp (by the overall increase of strength Z at higher q) and this will move the trajectory in the interior away from the (neighboring) fold caustic, so that lower flux will be predicted. Eventually, at sufficiently high q, the prediction will match the observations.

Hence, if there are two independent pieces of information from the remainder of the caustic, then this discrete degeneracy will almost always be broken (except for those due to deep symmetries, like $s \leftrightarrow s^{-1}$). For example, a caustic entrance would have four independent pieces of information. Inspection of Figure 4 shows that even one of these (such as the height or time of the entrance) would resolve the degeneracy. However, with only one piece

of information (as in the present case), the continuous degeneracies are broken but a discrete degeneracy is very likely.

From Figure 5, we see that the two minima have values of $\Delta\xi$ with opposite signs, meaning that the trajectories pass on opposite sides of the nominal center of the planetary caustic. That is, the trajectories have opposite chirality with respect to the caustic center. This feature is basically a product of the fact that the caustic exits must be on opposite sides of the minimum strength of the caustic wall. Hence, it is likely to be a generic (though probably not universal) feature of this degeneracy. For this reason, we dub this accidental degeneracy as the "caustic-chirality degeneracy".

4. Physical Parameters

Because ρ (or equivalently $t_* = \rho t_{\rm E}$) is measured, it will be possible to determine the lens-source relative proper motion $\mu = \theta_*/t_*$ and the angular Einstein radius,

$$\theta_{\rm E} \equiv \sqrt{\kappa M \pi_{\rm rel}}; \qquad \kappa \equiv \frac{4G}{c^2\,{\rm AU}} \simeq 8.14 \frac{\rm mas}{M_\odot}, \tag{2}$$

via $\theta_{\rm E} = \theta_*/\rho$. Here, M is the lens mass and $\pi_{\rm rel}$ is the lens-source relative parallax. Unfortunately, it is not possible to measure the microlens parallax $\pi_{\rm E}$ for this event, which would have permitted direct determination of the mass $M = \theta_{\rm E}/\kappa\pi_{\rm E}$ and $\pi_{\rm rel} = \theta_{\rm E}\pi_{\rm E}$ (Gould 1992, 2000). Hence it will be necessary to estimate these quantities from a Bayesian analysis.

4.1. Measurement of θ_*

To determine θ_* we first measure the offset of the source star from the Red Clump on an instrumental color-magnitude diagram. We find the color from regression of V on I flux based on the KMTC BLG41 data, which fortuitously has a point near the peak of the caustic exit. We find $\Delta(V-I) = -0.300 \pm 0.055$ for the color offset from the clump. Next, we find the offset in I-band magnitude by comparing the source flux in the instrumental system to that of the clump. Because there are two solutions that differ by $-2.5\log(f_{\rm s,A}, f_{\rm s,B}) = I_{\rm s,A} - I_{\rm s,B} = -0.174$, the offset from the clump will likewise differ by this amount. We find $\Delta I = +3.43 \pm 0.08$ (A) and $\Delta I = +3.60 \pm 0.08$ (B). That is, the source is likely to be a bulge turn-off star in either case. We adopt $[(V-I), I]_{\rm clump,0} = (1.06, 14.54)$ (Bensby et al. 2013; Nataf et al. 2013), to obtain $(V-I)_{s,0} = 0.76 \pm 0.06$ and $I_{s,0} = 17.97 \pm 0.09$ (A) and $I_{s,0} = 18.14 \pm 0.09$ (B). Then converting from $(V-I)$ to $(V-K)$ using the color-color relations of Bessell & Brett (1988) and applying the color/surface-brightness relations

of Kervella et al. (2004), we obtain

$$\theta_* = 0.845 \pm 0.079\,\mu\mathrm{as} \quad \text{(A)}; \qquad \theta_* = 0.781 \pm 0.073\,\mu\mathrm{as} \quad \text{(B)}. \tag{3}$$

4.2. Determination of $\theta_{\rm E}$ and μ

Applying Equation (3) and the results in Table 2, we then obtain

$$\theta_{\rm E} = \frac{\theta_*}{\rho} = 0.288 \pm 0.029\,\mathrm{mas} \quad \text{(A)}; \qquad \theta_{\rm E} = 0.317 \pm 0.035\,\mathrm{mas} \quad \text{(B)}. \tag{4}$$

and

$$\mu = \frac{\theta_*}{t_*} = 8.81 \pm 0.097\,\mathrm{mas\,yr^{-1}} \quad \text{(A)}; \qquad \mu = 8.91 \pm 0.098\,\mathrm{mas\,yr^{-1}} \quad \text{(B)}. \tag{5}$$

The relatively high proper motion is suggestive of a disk lens. If both the lens and the source were in the bulge, this would imply a relative velocity $\Delta v \simeq \mu D_S \simeq 350\,\mathrm{km\,s^{-1}}$, where we have adopted $D_s = 8.55\,\mathrm{kpc}$ for the source distance. This would be high, but certainly not impossible, given the one-dimensional dispersion of bulge lenses $\sigma_{\rm bulge} \sim 2.7\,\mathrm{mas\,yr^{-1}}$ derived from OGLE-IV measurements. On the other hand, the proper motions in Equation (5) would be quite typical of disk lenses.

However, the projected density of bulge stars is much higher than that of disk stars, which can partially compensate for the relatively poor match to bulge kinematics.

The Einstein radius places a joint constraint on the mass and relative parallax:

$$M = \frac{\theta_{\rm E}^2}{\kappa \pi_{\rm rel}} \rightarrow 0.11\,M_\odot \left(\frac{\pi_{\rm rel}}{0.10\,\mathrm{mas}}\right)^{-1}, \tag{6}$$

where we have made the evaluation using $\theta_{\rm E} \rightarrow 0.3\,\mathrm{mas}$ as a representative value, and where we have normalized to a "typical" relative parallax for a disk lens. Thus, because the proper motion provides only very weak constraints on the lens distance, we expect a very broad distribution of possible masses, centered on low-mass M dwarfs.

4.3. Bayesian Analysis

To make a more quantitative evaluation, we carry out a Bayesian analysis with the aid of a Han & Gould (1995) Galactic model. We draw sources and lenses randomly from the velocity and physical distributions of that model. For lenses, we draw according to $\nu(D_L) D_L^2 dD_L$ where D_L is the lens distance, but for sources we use $\nu(D_S) dD_S$ to account for

the lower frequency of more luminous sources (required to generate the observed source flux at greater distance). However, we find that this correction has a very small impact on the posterior distributions.. Our results are given in Table 3 for each of the two solutions. We note that the host mass and distance estimates are statistically indistinguishable between the two models, but the planet mass is a factor 2.2 higher in Local A, simply because q is higher by a similar factor.

Hence, as anticipated in Section 4.2, a quite broad range of host and planet masses are consistent with the microlensing solutions.

5. Discussion

The degeneracy presented here was relatively easy to discover because the χ^2 barrier between the two solutions is modest $\Delta\chi^2_{\rm barrier} \sim 9$ (see Figure 5). Hence, it can in principle appear in the course of running an MCMC to evaluate the error bars of the first solution that is found, or alternatively in a mildly hotter MCMC. This situation is more favorable for discovery than the case of OGLE-2017-BLG-0173, which had a much higher barrier (Hwang et al. 2018). However, this "favorable" circumstance is actually a by-product of unusually noisy KMTNet data for an event of this brightness. The source star happened to lie below two relatively bright stars on the CCD, which bled by small amounts onto the point spread function (PSF) of the source. If this were not the case, the error bars would have been smaller by a factor ~ 1.7, implying that $\Delta\chi^2_{\rm barrier}$ would have been ~ 3 times higher.

Thus, as in the cases outlined in Section 1, it is important to have an analytic understanding of this degeneracy in order to recognize when it might be present and to know how to look for it. We have provided such guidelines in Section 3.3.

5.1. Future Resolution

Future high-resolution images can clearly resolve the uncertainties in the host mass and distance that were evaluated in Section 4.3, but the problem of breaking the factor ~ 2.5 discrete degeneracy in q (and so in planet mass) is considerably more challenging.

Using Keck adaptive optics (AO), Batista et al. (2015) fully resolved the source and lens of OGLE-2005-BLG-169 when they were separated by ~ 60 mas, and Bennett et al. (2015) partially resolved them when they were separated by ~ 50 mas using the *Hubble Space Telescope (HST)*. That case was somewhat more favorable than the present one because the source and lens had comparable fluxes, whereas for OGLE-2017-BLG-0373 the lens could be

substantially fainter than the source. Therefore, to be conservative, we can estimate that full resolution with presently existing instruments should be possible when the separation is $\sim 90\,\mathrm{mas}$. Given that the proper motion is $\mu \sim 9\,\mathrm{mas\,yr^{-1}}$, such imaging could be done 10 years after the event. Combining such imaging with the mass-distance relation for the host derived from the θ_E measurement (Equation (6)) would lead to a precise host-mass measurement as it did for OGLE-2005-BLG-169.

There is also the potential for future high-resolution imaging to resolve the discrete degeneracy between solutions A and B. From Table 2, these two solutions predict I-band magnitudes that differ by $I_{\mathrm{s,A}} - I_{\mathrm{s,B}} = -0.174 \pm 0.067$. This is a 2.6σ difference, so in principle if the source flux were accurately measured in future high-resolution images, this could resolve the mass-ratio degeneracy with reasonable confidence[2]. Unfortunately, our measurement of the source color (Section 4.1) was relatively imprecise, which implies that to determine the I-band magnitude, one must make the measurement in a bandpass near I-band and also measure the source flux in a second relatively nearby bandpass to determine the color. Then one would be able to accurately estimate I_s using color-color relations based on field stars. Hence, this measurement probably requires either *HST*, which will probably be decommissioned by that time, or the *James Webb Space Telescope*, assuming that the latter is successfully launched and remains operational.

The OGLE project has received funding from the National Science Centre, Poland, grant MAESTRO 2014/14/A/ST9/00121 to AU. Work by WZ, YKJ, and AG were supported by AST-1516842 from the US NSF. WZ, IGS, and AG were supported by JPL grant 1500811. This research has made use of the KMTNet system operated by the Korea Astronomy and Space Science Institute (KASI) and the data were obtained at three host sites of CTIO in Chile, SAAO in South Africa, and SSO in Australia. Work by YS was supported by an appointment to the NASA Postdoctoral Program at the Jet Propulsion Laboratory, California Institute of Technology, administered by Universities Space Research Association through a contract with NASA. Work by C. Han was supported by grant (2017R1A4A1015178) of the National Research Foundation of Korea.

[2]In order to enable such an excercise, the photometry of neighbouring stars (in the same photometric system than the light curve) will be submitted to NASA Exoplanet Archive and available from https://exoplanetarchive.ipac.caltech.edu/.

REFERENCES

Albrow, M. D., Horne, K., Bramich, D. M., et al. 2009, MNRAS, 397, 2099

Alcock, C., Alssman, R.A., Alves, D.R., et al. 2001, Nature, 414, 617

Alard, C. & Lupton, R.H.,1998, ApJ, 503, 325

An, J.H. et al. 2005, MNRAS, 356, 1409

Batista, V., Beaulieu, J.-P., Bennett, D.P., et al. 2015, ApJ, 808, 170

Beaulieu, J.-P. Bennett, D.P., Fouqué, P. et al. 2006, Nature, 439, 437

Bennett, D.P., Bhattacharya, A., Anderson, J., et al. 2015, ApJ, 808, 169

Bensby, T. Yee, J.C., Feltzing, S. et al. 2013, A&A, 549A, 147

Bessell, M.S., & Brett, J.M. 1988, PASP, 100, 1134

Dominik, M. 1999, A&A, 349, 108

Gaudi, B.S. 1998, ApJ, 506, 533

Gould, A. 1992, ApJ, 392, 442

Gould, A. 2000, ApJ, 582, 785

Gould, A. 2004, ApJ, 606, 319

Gould, A. 2008, ApJ, 681, 1593

Gould, A. & Andronov, N. 1999, ApJ, 516, 236

Gould, A. & Loeb, A. 1992, ApJ, 396, 104

Gould, A., Carey, S., & Yee, J. 2016, spitz.prop 13005

Griest, K. & Safizadeh, N. 1998, ApJ, 500, 37

Han, C. 2006, ApJ, 638, 1080

Han, C. & Gould, A. 1995, ApJ, 447, 53

Hwang, K.-H., Udalski, A., Bond, I.A., et al. 2017, AAS journals, submitted, arXiv:1711.09651

Hwang, K.-H., Udalski, A., Shvartzvald, Y. et al. 2018, AJ, 155, 22

Kayser, R., Refsdal, S., & Stabell, R. 1986, A&A, 166, 36

Kervella, P., Thévenin, F., Di Folco, E., & Ségransan, D. 2004, A&A, 426, 297

Kim, S.-L., Lee, C.-U., Park, B.-G., et al. 2016, JKAS, 49, 37

Nataf, D.M., Gould, A., Fouqué, P. et al. 2013, ApJ, 769, 88

Paczyński, B. 1986, ApJ, 304, 1

Park, H., DePoy, D.L., Gaudi, B.S., et al. 2004, ApJ, 609, 166

Pejcha, O., & Heyrovský, D. 2009, ApJ, 690, 1772

Schneider, P., & Weiss, A. 1988, ApJ, 330, 1

Skowron, J., Udalski, A., Gould, A et al. 2011, ApJ, 738, 87

Smith, M., Mao, S., & Paczyński, B., 2003, MNRAS, 339, 925

Udalski, A. 2003, Acta Astron., 53, 291

Udalski, A.,Szymanski, M., Kaluzny, J., et al. 1994, Acta Astron., 44, 227

Wambsganss, J. 1997, MNRAS, 284, 172

Woźniak, P. R. 2000, Acta Astron., 50, 421

Udalski, A., Szymański, M.K. & Szymański, G. 2015, Acta Astronom., 65, 1

Udalski, A.,Ryu, Y.-H., Sajadian, S., et al. 2018,submitted, arXiv:1802.02582

Table 1. Five Candidate Models

Model	s	q	χ^2
Local A	1.38	0.0015	2795.0
Model 1	0.79	0.056	2890.9
Model 2	0.80	0.0009	2893.8
Model 3	1.15	0.033	2944.8
Model 4	0.77	0.019	2967.4

Table 2. Best-fit solutions

Parameters	Local A	Local B
χ^2/dof	2795.00/2795	2795.22/2795
t_0 (HJD′)	7840.607 ± 0.054	7840.636 ± 0.054
u_0	0.416 ± 0.011	0.371 ± 0.015
$t_{\rm E}$ (days)	11.993 ± 0.243	12.849 ± 0.349
s	1.376 ± 0.010	1.349 ± 0.011
q (10^{-3})	1.544 ± 0.352	0.651 ± 0.113
α (rad)	2.461 ± 0.015	2.465 ± 0.011
ρ (10^{-3})	2.935 ± 0.190	2.466 ± 0.201
f_S	0.263 ± 0.009	0.224 ± 0.012
f_B	1.086 ± 0.009	1.125 ± 0.012
t_* (days)	0.035 ± 0.002	0.032 ± 0.002
$t_{\rm eff}$ (days)	4.988 ± 0.089	4.765 ± 0.100

Note. — The fluxes f_S and f_B are normalized to $I = 18$.

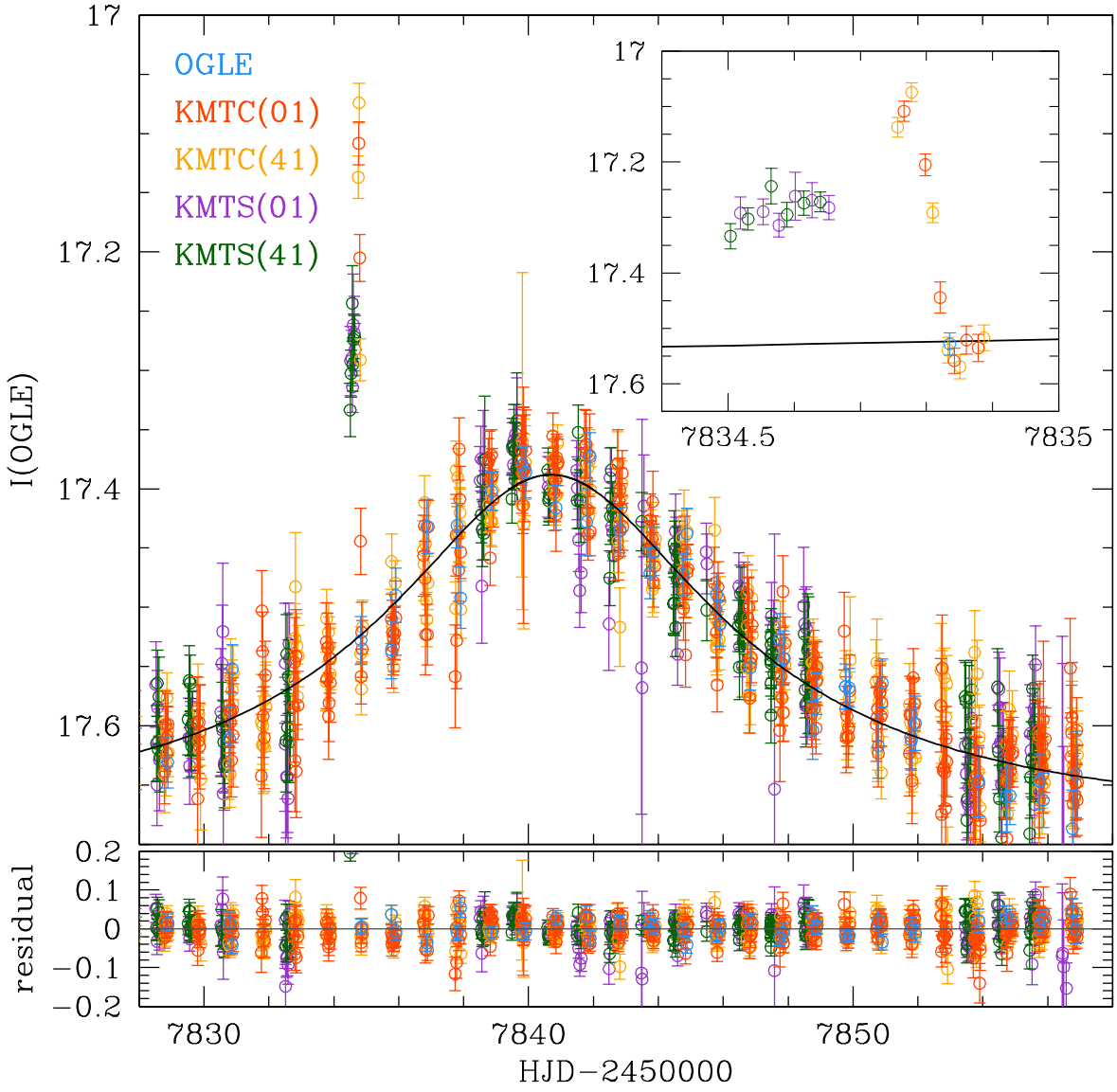

Fig. 1.— Light curve and point-lens (Paczyński 1986) model for OGLE-2017-BLG-0373. The data points are color-coded by observatory and field. The inset shows the anomaly. Even without a model, it is clear that this is a caustic trough followed by a caustic exit. While this morphology is eerily reminiscent of (a time reversal of) Gould & Loeb (1992)'s original illustration of planetary-caustic microlensing, it is actually broadly consistent with five different binary-microlensing topologies, which must be systematically vetted. See Figure 2.

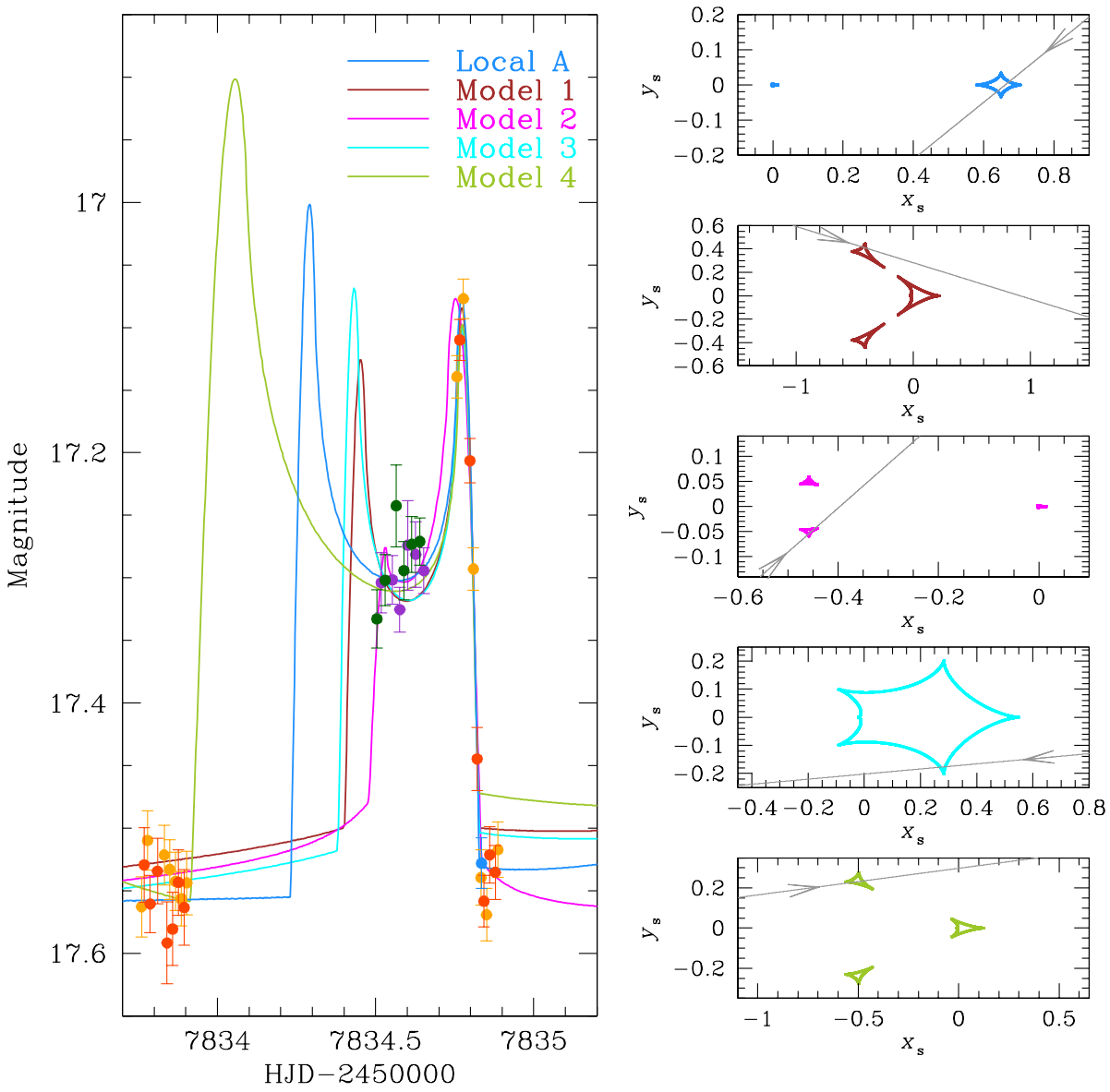

Fig. 2.— Models derived from five different binary-lens topologies that roughly fit the lightcurve of OGLE-2017-BLG-0373. All look roughly plausible, but one of them (the major-image planetary-caustic model (Local A) is favored over all the others by $\Delta\chi^2 \gtrsim 100$. See Table 1. The caustic geometries for the models are shown in the five right-hand panels, with the caustics color-coded to match the models in the left-hand panel. Note that all of the caustic diagrams are drawn to the same scale.

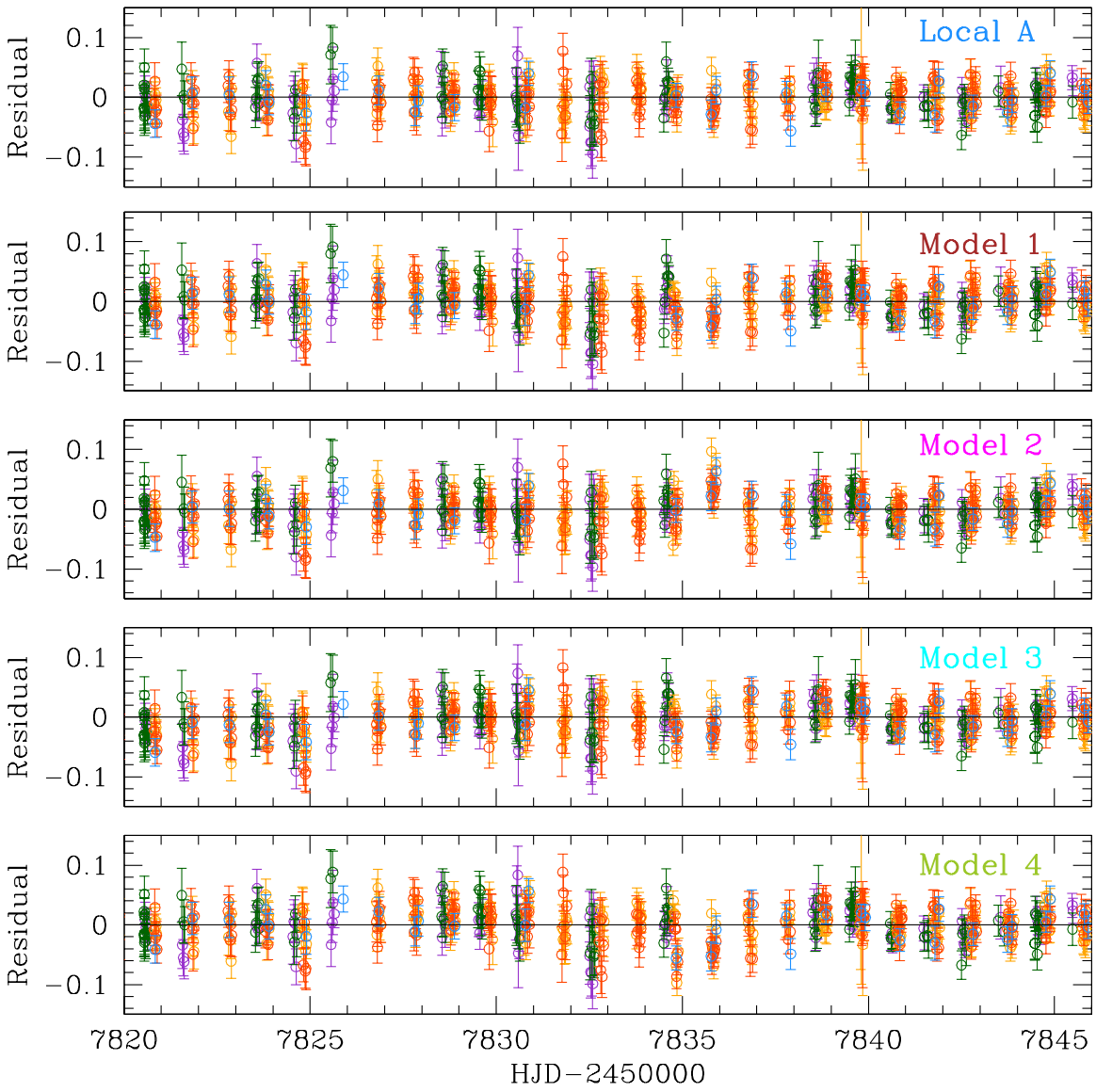

Fig. 3.— Residuals for the five models shown in Figure 2. Model 1 and Model 3 fail primarily because of week-long systematic residuals centered on HJD′ ∼ 7834 and ∼ 7823, respectively. Models 2 and 4 fail primarily due to concentrated deviations on and/or immediately after the caustic exit. The peak of the event is $t_0 \sim 7840.6$ and anomaly is at $t \sim 7834.5$.

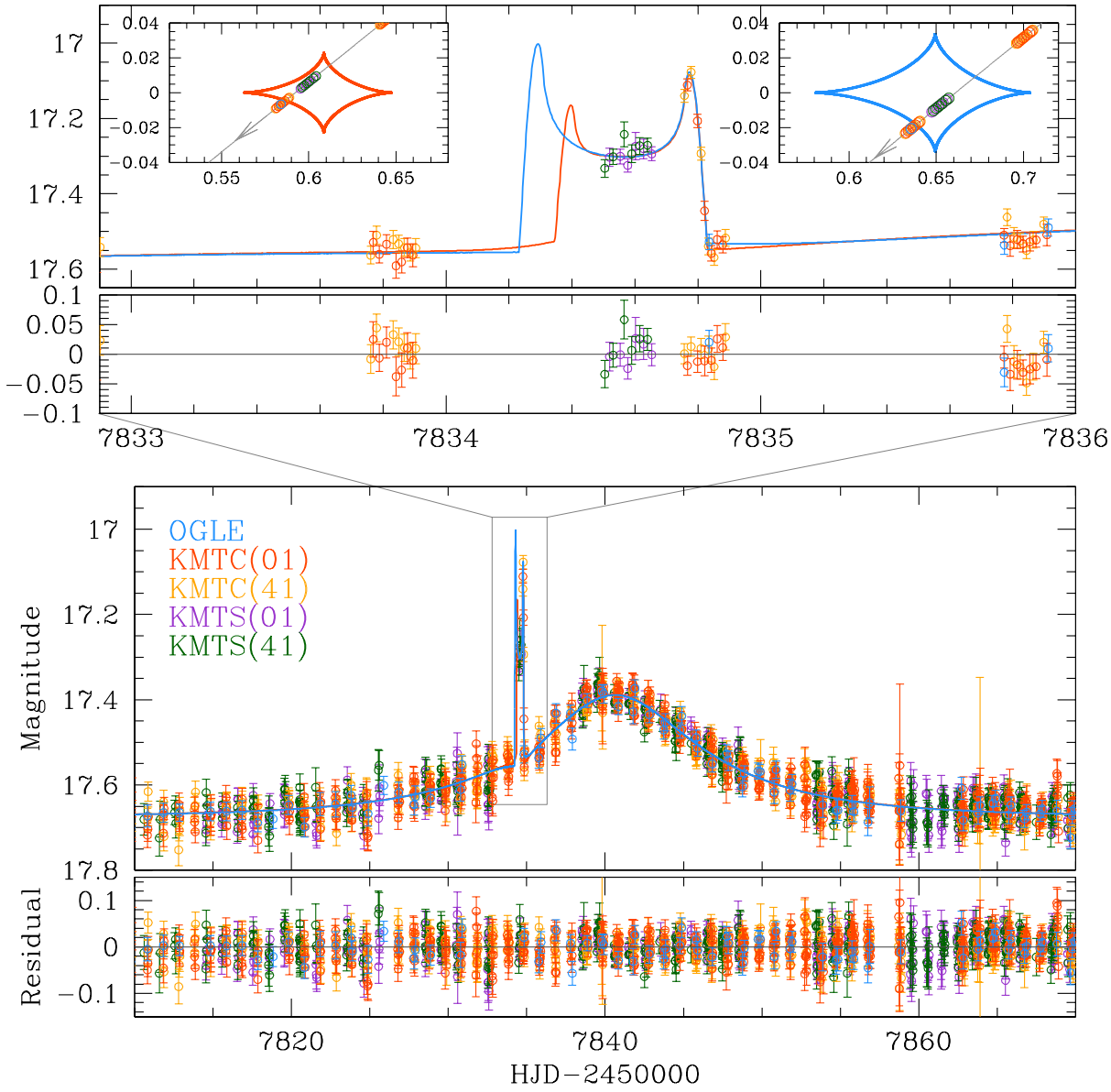

Fig. 4.— Two models compared to the data for OGLE-2017-BLG-0373. The two models, which have extremely similar parameters except for a factor 2.5 difference in mass-ratio q, fit the data equally well. This degeneracy is accidental in the sense that additional data over the caustic entrance would clearly have distinguished between them. The caustic diagrams for each model are shown in the insets with the same color coding as the model light curves.

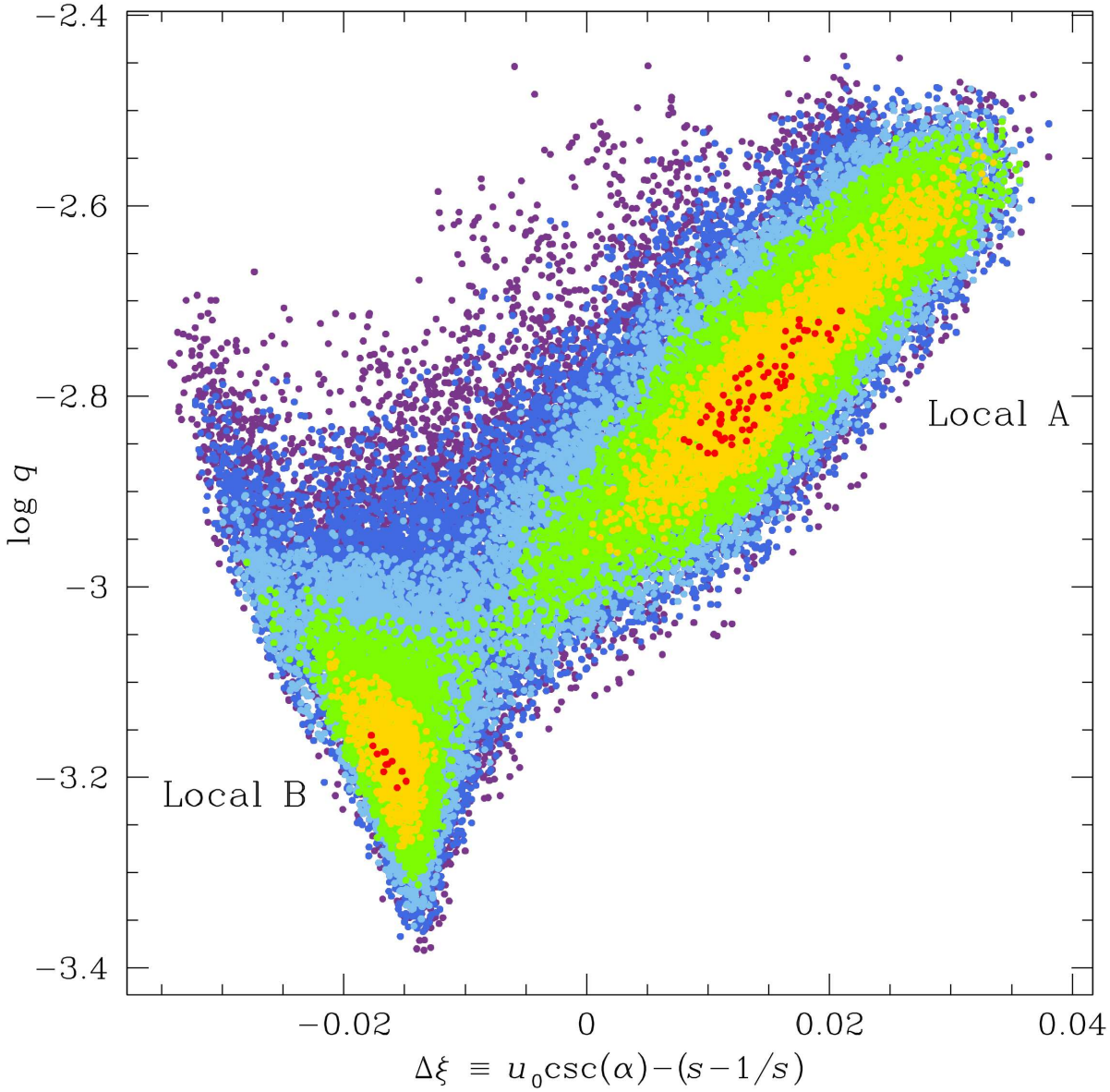

Fig. 5.— χ^2 distribution over the plane of $\log q$ versus $\Delta\xi \equiv u_0 \csc\alpha - (s - s^{-1})$, where $\Delta\xi$ is the offset between the source and the center of the caustic at the time that the source crosses the binary axis. Red, yellow, green, cyan, blue, and purple represent $\Delta\chi^2 < 1, 4, 9, \ldots 36$. The two models have virtually identical χ^2 but are separated by a barrier $\Delta\chi^2_{\rm barrier} \sim 9$. The origin of this structure is investigated in Section 3.3.

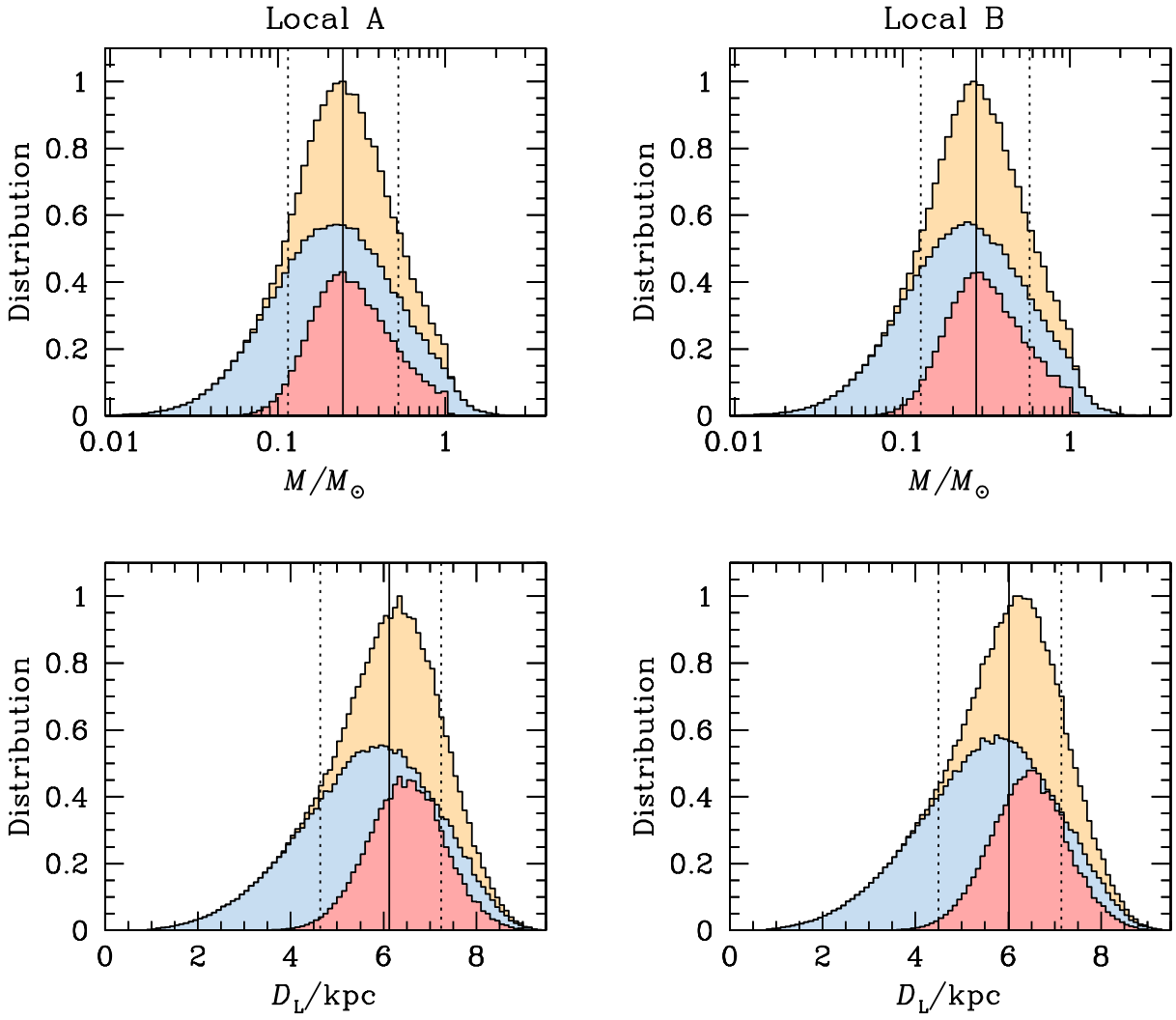

Fig. 6.— Posterior distributions of the host mass and system distance of OGLE-2017-BLG-0373Lb, which prove to be nearly identical for the two degenerate solutions, A and B. The total probability distribution (gold) is divided into disk (blue) and bulge (red) lenses. The median (50%), 16%, and 84% percentiles are shown. The true values of these host properties can easily be determined from high-resolution imaging ~ 10 years after the event. However, resolving the factor 2.5 mass-ratio degeneracy between the two models will be more challenging. See text.

Table 3. PHYSICAL PROPERTIES

Quantity	Local A	Local B
$M_{\rm host}$ $[M_\odot]$	$0.248^{+0.274}_{-0.133}$	$0.276^{+0.296}_{-0.148}$
$M_{\rm planet}$ $[M_J]$	$0.401^{+0.637}_{-0.257}$	$0.189^{+0.270}_{-0.116}$
$D_{\rm L}$ [kpc]	$5.915^{+1.123}_{-1.478}$	$5.810^{+1.133}_{-1.523}$
$a_\perp$ [au]	$2.424^{+0.757}_{-0.783}$	$2.575^{+0.850}_{-0.878}$